Simulation and mitigation of noise in Rydberg atom systems using quantum optimal control

by

Caroline Laure MBAKOB TCHOUAWOU

A thesis
presented to the University of Waterloo
in fulfillment of the
thesis requirement for the degree of
Master of Science
in
Physics (Quantum Information)

Waterloo, Ontario, Canada, 2021

Author's Declaration

I hereby declare that I am the sole author of this thesis. This is a true copy of the thesis, including any required final revisions, as accepted by my examiners.

I understand that my thesis may be made electronically available to the public.

Abstract

In this thesis, we design a quantum optimal control protocol to mitigate the noise in Rydberg atom systems. First, we address the problem of simulating the dynamics of a single rubidium-87 atom excited to a Rydberg state in the presence of imperfections. Then, we design an optimal control protocol to mitigate the effect of physical imperfections and fluctuations in control parameters. This work will be useful for applications in quantum information processing and quantum simulation.

Acknowledgements

"Teach your students to doubt, to think, to communicate, to question, to make mistakes, to learn from their mistakes and most importantly have fun in their learning." It is with those words from Richard Feynman that I would like to thank:

First and foremost, my supervisor David Cory for giving me the opportunity to work and study in his group. The group discussions we had each week broadened my knowledge and expertise in the areas of quantum information and quantum control.

I would like to thank Jeremy Levick from AIMS who introduced me to the field of quantum computing.. My deepest and sincere thank to Alexandre Cooper-Roy for the devotion, time and energy that he has invested to establish the Quantum Simulation Group in Cory's Lab. Working with him was one of the greatest experience in my life. The methodology he used for me to come up with this thesis will always stay in my mind. I am also so grateful to Jeremy Flannery, who gave me the possibility to deeply understand quantum concepts; I am so thankful for the great mentor he is.

I would like to thank the Quantum Simulation Group in Cory's Lab. The insightful discussions among us helped me a lot to enjoy my learning experience. Thank also to members of David Cory's group, especially Troy Borneman, Maryam Mirkamali who introduced me to quantum information.

I would like to thank all my University of Waterloo lecturers, especially Joseph Emerson, Dmitry Pushin, John Yard, Raymond Laflamme, and Chris Wilson. Their lectures helped me to better understand many new quantum information concepts.

I would not end without sending my great sincere thank to my family for their prayers, support, love, advice. I thank also my friends Gole, Kongho, Inoussa for their support.

Dedication

I dedicate this thesis to my family especially to my mother.

Table of Contents

List of Tables

List of Figures

Chapter 1

Simulating the dissipative dynamics of an effective two–level system

This thesis addresses the problem of improving the performance of quantum simulators using quantum optimal control. In particular, this thesis addresses the problem of exciting a neutral atom to a Rydberg state using optimal control pulses to mitigate the effect of dissipative physical processes and fluctuations in control parameters.

1.1 Thesis outline and summary of contributions

In Chapter 1, we address the problem of simulating the dynamics of a single rubidium-87 atom excited to a Rydberg state via a two-photon transition in the presence of fluctuating control parameters. First, we introduce the control problem and describe experimental imperfections. Then, we show that the dynamics of a three-level system can be approximated by the dynamics of an effective two-level system. Finally, we simulate the dynamics of the effective two-level system in the presence of amplitude and phase noise in the control lasers. These results establish the protocol to design optimal control pulses to mitigate these imperfections.

In Chapter 2, we address the problem of using optimal control pulses to counteract dissipation and fluctuations in control parameters. First, we introduce two control protocols to increase the fidelity of excitation of a single rubidium atom to a Rydberg state: stimulated Raman adiabatic passage (STIRAP) and superadiabatic transitionless driving (SATD). Then, we show that these control protocols increase the fidelity of a rubidium atom excited to a Rydberg state. Finally, we design a robust control pulse using quantum optimal control and compare its result to the STIRAP and the SATD protocols.

1.2 Description of the control problem

Quantum simulators enable exploring the dynamics of quantum many-body systems [1–10]. A promising platform for quantum simulation is neutral atoms trapped in arrays of optical tweezers interacting via Rydberg-mediated interactions [1–3, 8, 10–16]. Here, we

consider rubidium–87 (Rb–87) atoms trapped in arrays of optical tweezers. The atoms are coherently controlled using laser beams and microwave fields. A tunable interaction is introduced by exciting atoms to a Rydberg state, which then acquire unique physical properties (Table 1.1).

Properties	symbols	Rydberg atoms's properties as function of their quantum number n	typical value for $70S_{1/2}$ of Rb–87
Binding energy	E_n	n^{-2}	-500 GHz
Level spacing	$E_{n+1} - E_n$	n^{-3}	$[10 - 100]$ GHz
Size of wave function	$\langle r \rangle$	n^2	500 nm
Lifetime	τ	n^3	100 μs
Polarizability	α	n^7	-1.5 GHz/(V/cm)^2
van der Waals coefficient	C_6	n^{11}	10 THz. μm^6

Table 1.1: Physical properties of Rydberg atoms. Properties of Rb–87 atoms excited to a Rydberg state as a function of their primary quantum number n with their experimental values reported for $70S_{1/2}$.

1.2.1 Rubidium–87 atoms

Our controllable quantum system is formed by a Rb-87 addressed optically using laser beams. The relevant energy levels of Rb–87 form a three-level system (Fig. 1.1). The ground state is chosen as the hyperfine state, $|g\rangle = |5S_{1/2}, F = 2, m_F = -2\rangle$ and the excited state is chosen as the Rydberg state, $|r\rangle = |70S_{1/2}, m_J = -1/2\rangle$. Because the direct optical excitation from $|g\rangle$ to $|r\rangle$ is forbidden by selection rules, we excite the atoms from the ground state $|g\rangle$ to the excited state $|r\rangle$ via the intermediate state $|i\rangle = |6P_{3/2}, F = 3, m_F = -3\rangle$.

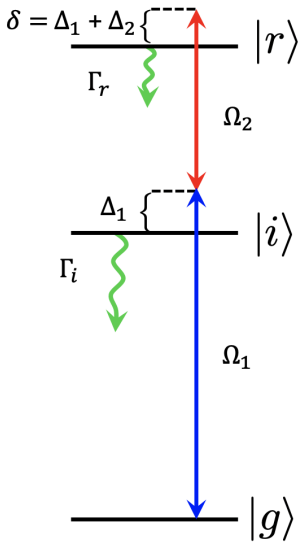

Figure 1.1: Relevant energy levels of a Rb-87 atom with optical transitions. The optical transition (blue double arrows) from the ground state $|g\rangle = |5S_{1/2}, F = 2, m_F = -2\rangle$ to the intermediate state $|i\rangle = |6P_{3/2}, F = 3, m_F = -3\rangle$ is driven with a laser beam at $\lambda_1 = 420$ nm with circular polarization σ_-. The Rabi frequency is Ω_1 and the frequency detuning is Δ_1. The optical transition (red double arrows) from the intermediate state $|i\rangle = |6P_{3/2}, F = 3, m_F = -3\rangle$ to the Rydberg state $|r\rangle = |70S_{1/2}, m_J = -1/2\rangle$ is driven with a laser beam at $\lambda_2 = 1013$ nm with circular polarization σ_+. The Rabi frequency is Ω_2 and the frequency detuning is Δ_2. The two-photon detuning is $\delta = \Delta_1 + \Delta_2$. The decay rate (green long wiggly arrow) of the intermediate state is $\Gamma_i = 2\pi \times 0.282$ MHz [17]. The decay rate (green small wiggly arrow) to the Rydberg state is $\Gamma_r = 2\pi \times 2.67$ kHz.

1.2.2 Master equation

The master equation describes the dissipative evolution of a quantum system. It is described by its Hamiltonian $\mathcal{H}$ and its dissipator $\mathcal{L}$. The Hamiltonian describes the interaction of the atom with the laser field, whereas the Lindbladian describes the noise acting on the system under the Markovian approximation.

The interaction of the three-level system and the laser field is described by the Markovian master equation (1.1) for the unknown density matrix ρ,

$$\frac{d\rho}{dt} = \frac{1}{i\hbar}[\mathcal{H}, \rho] + \mathcal{L}[\rho], \tag{1.1}$$

where the Hamiltonian $\mathcal{H}$ is

$$\mathcal{H} = -\Delta_1(|i\rangle\langle i|) - \delta(|r\rangle\langle r|) + \frac{\Omega_1}{2}(|g\rangle\langle i| + |i\rangle\langle g|) + \frac{\Omega_2}{2}(|i\rangle\langle r| + |r\rangle\langle i|), \tag{1.2}$$

and the dissipator $\mathcal{L}$ is

$$\mathcal{L}[\rho] = \frac{\Gamma_i}{2}(2|g\rangle\langle i|\rho|i\rangle\langle g| - |i\rangle\langle i|\rho - \rho|i\rangle\langle i|) + \frac{\Gamma_r}{2}(2|i\rangle\langle r|\rho|r\rangle\langle i| - |r\rangle\langle r|\rho - \rho|r\rangle\langle r|), \tag{1.3}$$

where $\Gamma_i = 2\pi \times$ 0.282 MHz [17] and $\Gamma_r = 2\pi \times 2.67$ kHz are the decay rates of the intermediate and the Rydberg states respectively. Here, we have made the assumption that the first laser field does not drive the second optical transition and the second laser field does not drive the first optical transition.

Our time–dependent observable is the population of the Rydberg state $P_r(t)$. Our measurement operator Π_r is the projector on the Rydberg state $|r\rangle$, $\Pi_r = |r\rangle\langle r|$. The time–dependent population $P_r(t)$ of the Rydberg state is thus

$$P_r(t) = \mathrm{Tr}\{\rho(t)\Pi_r\}. \tag{1.4}$$

1.2.3 Dynamics of a three–level system

Given the initial state $\rho(0) = |g\rangle\langle g|$, we compute the time–evolved state $\rho(t)$ by solving the master equation (1.1) using the Qutip library (version 4.6.0) in Python (version 3.7). The intermediate state has a short lifetime, leading to a reduced excitation probability to the Rydberg state. To increase the excitation probability, the first driven field is detuned away from the intermediate state $|i\rangle$ (Fig. 1.2a). To reduce scattering off the intermediate state, we choose the detuning of the first laser to be $\Delta_1 = 2\pi \times 740$ MHz and the detuning of the second laser to be $\Delta_2 = -\Delta_1$, so that the two–photon detuning is $\delta = 0$ kHz to avoid spontaneous decay on the Rydberg state. The excitation probability to the Rydberg state increases with the detuning until decay from the Rydberg state dominates the dynamics (Fig. 1.2b).

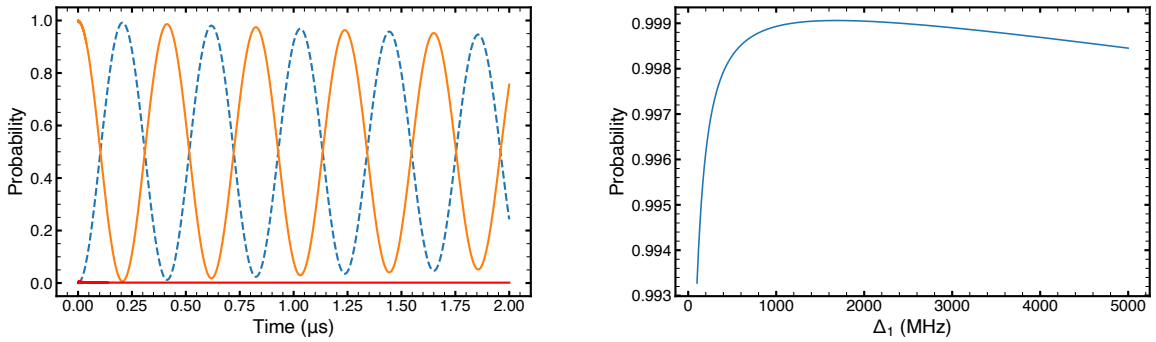

(a) **(b)**

Figure 1.2: Probability of exciting a single–atom to a Rydberg state. (a) Excitation probability of the ground state (orange solid line) to the Rydberg state (blue dash line) via the intermediate state (red solid line) for $\Delta_1 = 2\pi \times$ 740 MHz. (b) Excitation probability of the Rydberg state at $t = (2\pi/\Omega)$ μs, where $\Omega = \Omega_1\Omega_2/2\Delta_1$. The excitation probability to the Rydberg state increases with the detuning away from the intermediate state until the decay from the Rydberg state limits the excitation probability.

1.2.4 Dynamics of an effective two–level system

In the limit of large detunings Δ_1 from the intermediate state, the dynamics of the three–level system can be approximated by the effective Hamiltonian

$$\mathcal{H}_{eff} = -\Delta_{eff}|r\rangle\langle r| + \frac{\Omega_{eff}}{2}(|g\rangle\langle r| + |r\rangle\langle g|), \tag{1.5}$$

where $\Omega_{\text{eff}} = \Omega_1\Omega_2/2\Delta_1$ is the effective two–level system drive field, $\Delta_{\text{eff}} = -\delta - \Delta_{AC}$ is the effective detuning, and $\Delta_{AC} = -(\Omega_1^2 - \Omega_2^2)/4\Delta_1$ is the AC stark shift arising from the interaction of the intermediate state with a far–detuned driving field.

The dissipator for a Markovian noise takes the form

$$\mathcal{L}[\rho] = \frac{\Gamma_{eff}}{2}(2|g\rangle\langle r|\rho|r\rangle\langle g| - |r\rangle\langle r|\rho - \rho|r\rangle\langle r|), \tag{1.6}$$

where

$$\Gamma_{eff} = \Gamma_r + \Gamma_i\frac{\Omega_1^2 + \Omega_2^2}{4\Delta_1^2} \tag{1.7}$$

is the effective two–level decay rate. We confirm that the effective two–level dynamics matches the three–level dynamics in the far–detuned regime (Fig. 1.3).

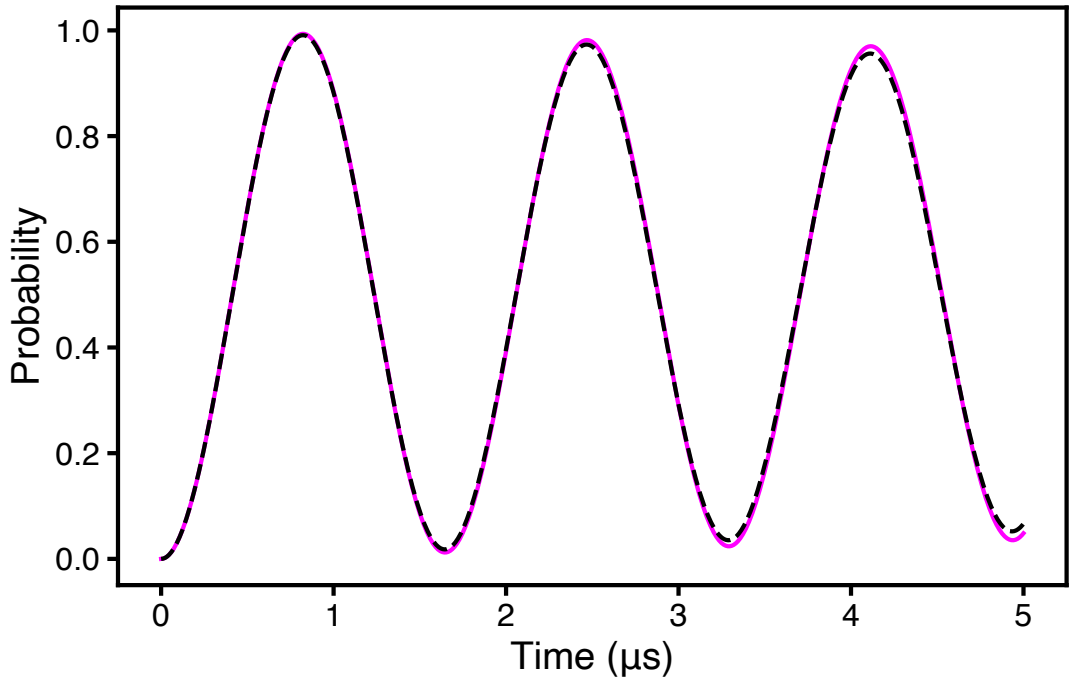

Figure 1.3: Rabi oscillations for the effective two–level system. Comparison of the simulated dynamics for the three–level system (black dash line) and the effective two–level system (pink solid line). We confirm that the effective two–level dynamics matches the three–level dynamics in the far–detuned regime. The simulation parameters are $\Delta_1 = 2\pi \times 740$ MHz, $\delta = 2\pi \times 0$ kHz, $\Omega_1 = 2\pi \times 60$ MHz, and $\Omega_2 = 2\pi \times 60$ MHz.

1.2.5 Dynamics of an effective two–level system with dissipation

We now simulate the dissipative evolution caused by two sources of imperfections: dissipative physical parameters and fluctuating control parameters. Because the quantum dynamics resulting from those fluctuating control parameters is a non–Markovian process, we simulate the quantum dynamics using the Monte Carlo sampling method, i.e., by averaging the solution of the master equation over multiple realizations of the noise rather than using a Lindbladian.

1.2.5.1 Dissipative physical processes

Imperfections in the physical system include radiative decay, black–body radiation, and Doppler effect.

- **Radiative decay**

  Given an atom in an excited state, there is a probability for the atom to return to a lower energy state by releasing a photon. This phenomenon is called spontaneous emission. In our system, the rate of decay of the intermediate state and the Rydberg state is Γ_i and Γ_r respectively. The effect of spontaneous emission in the Rydberg state is seen in Figure 1.3, where $\Gamma_i = 2\pi \times 0.282$ MHz [17] and $\Gamma_r = 2\pi \times 2.67$ kHz.

- **Black–body radiation (BBR)**

  According to Planck, the energy B_ν released from a black–body at temperature T is

  $$B_\nu(\nu, T) = \frac{2h\nu^3}{c^2} \frac{1}{e^{\frac{h\nu}{k_B T}} - 1}, \tag{1.8}$$

  where ν the frequency of the electromagnetic radiation, c the speed of light in the vacuum, k_B the Boltzmann constant, and h the Planck constant. In our system, at large quantum number $n \approx 70$, the depopulation rate of the Rydberg state due to the BBR decreases at large quantum number n (Fig 1.4).

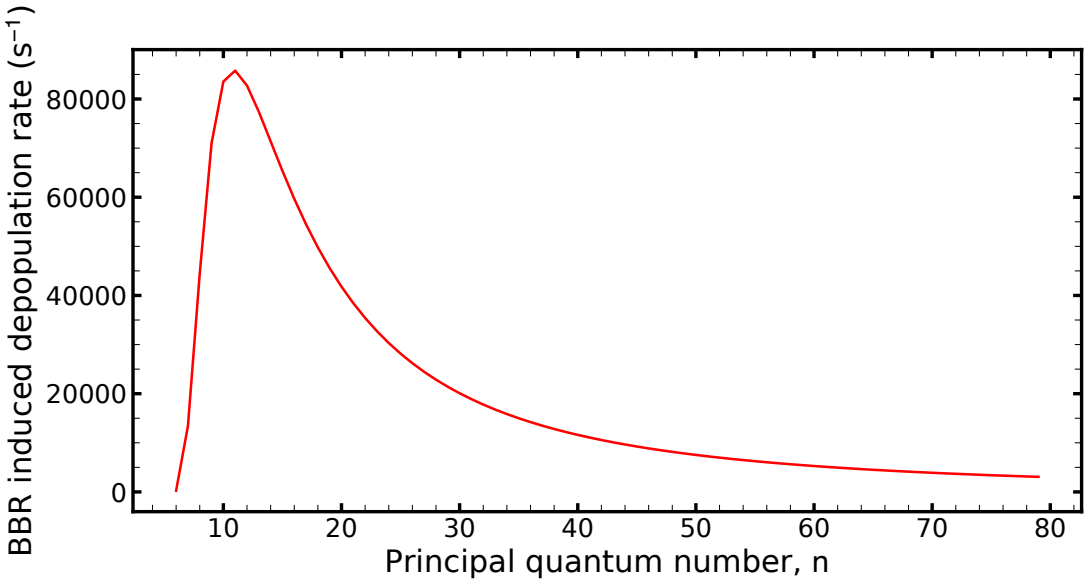

Figure 1.4: Depopulation rate induced by black–body radiation. At large quantum number, the effect of the BBR on the depopulation of the Rydberg state is small compared to the radiative decay, $\Gamma_r = 2\pi \times 2.67$ kHz.

- **Doppler effect**

  The Doppler effect is associated with the change of the frequency effectively seen in the reference frame of the atom due to its velocity. In our system, we use two counter–propagating beams with wavevectors $\vec{k}_{1013}$ and $\vec{k}_{420}$. The effective frequency seen in the reference frame of the atom is $k_{eff} = k_{420} - k_{1013}$, where $k = 2\pi/\lambda$. At temperature T, the spread in velocity of the atoms is $\Delta v = \sqrt{\frac{k_B T}{m}}$ and its standard deviation is $k_{eff}\Delta v$. In the reference frame of the atom, the Doppler effect leads to a fluctuation of the two–photon detuning δ (Fig. 1.5).

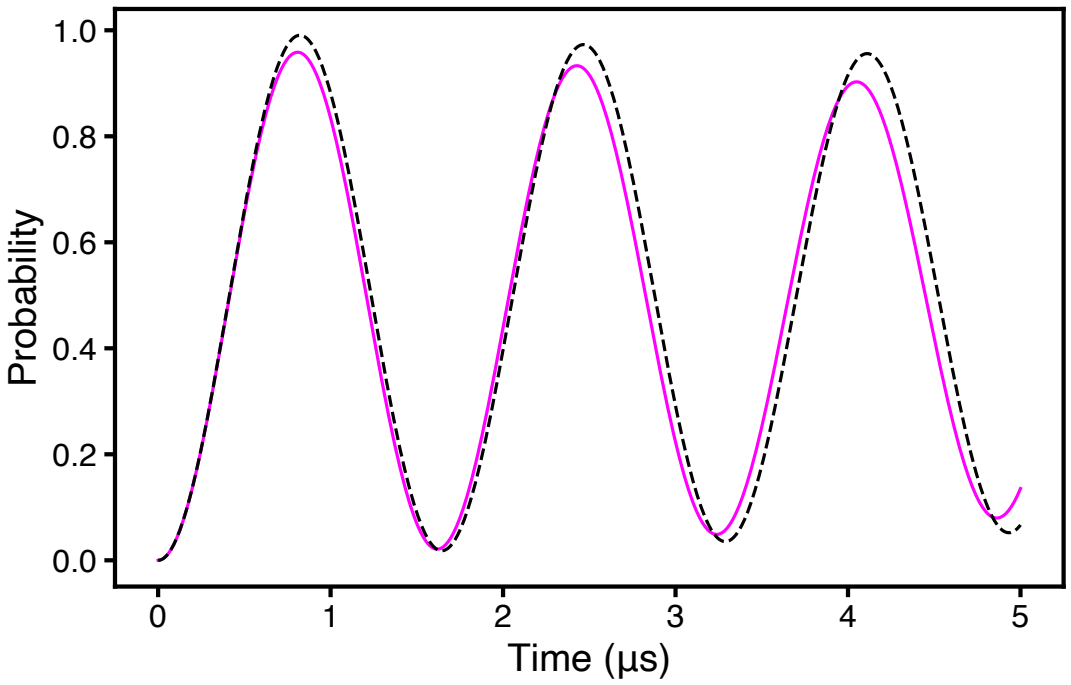

Figure 1.5: Doppler effect. Probability to reach the Rydberg state for $k_{eff}\Delta\nu = 2\pi \times 120$ kHz (pink solid line) and $k_{eff}\Delta\nu = 2\pi \times 10$ kHz (black dash line). An increase of the mean temperature leads to a decrease in the population of the Rydberg state. These results were obtained for $\Delta_1 = 2\pi \times 740$ MHz, $\delta = 2\pi \times 0$ kHz, $\Omega_1 = 2\pi \times 30$ MHz, $\Omega_2 = 2\pi \times 30$ MHz, $k_{eff} = 8.76 \times 10^6\ m^{-1}$, and $T = 30\ \mu K$.

1.2.5.2 Fluctuations in control parameters

We now consider the effect of amplitude noise and phase noise on the dynamics of the effective two–level system.

The phase noise of the laser can be measured by beating the laser against a more stable laser reference. If such a reference is not available, the phase noise of the laser can be inferred from the fluctuations in the error signal of the servo controller stabilizing the laser to the reference cavity. For our calculations, we use the phase noise data extracted from Ref. [13], which provided phase noise data for a two–photon transition driven at 795 nm and 475 nm. Because the laser light at 475 nm is obtained from frequency doubling of a laser source at 950 nm, the phase noise is specified for the fundamental laser at 950 nm.

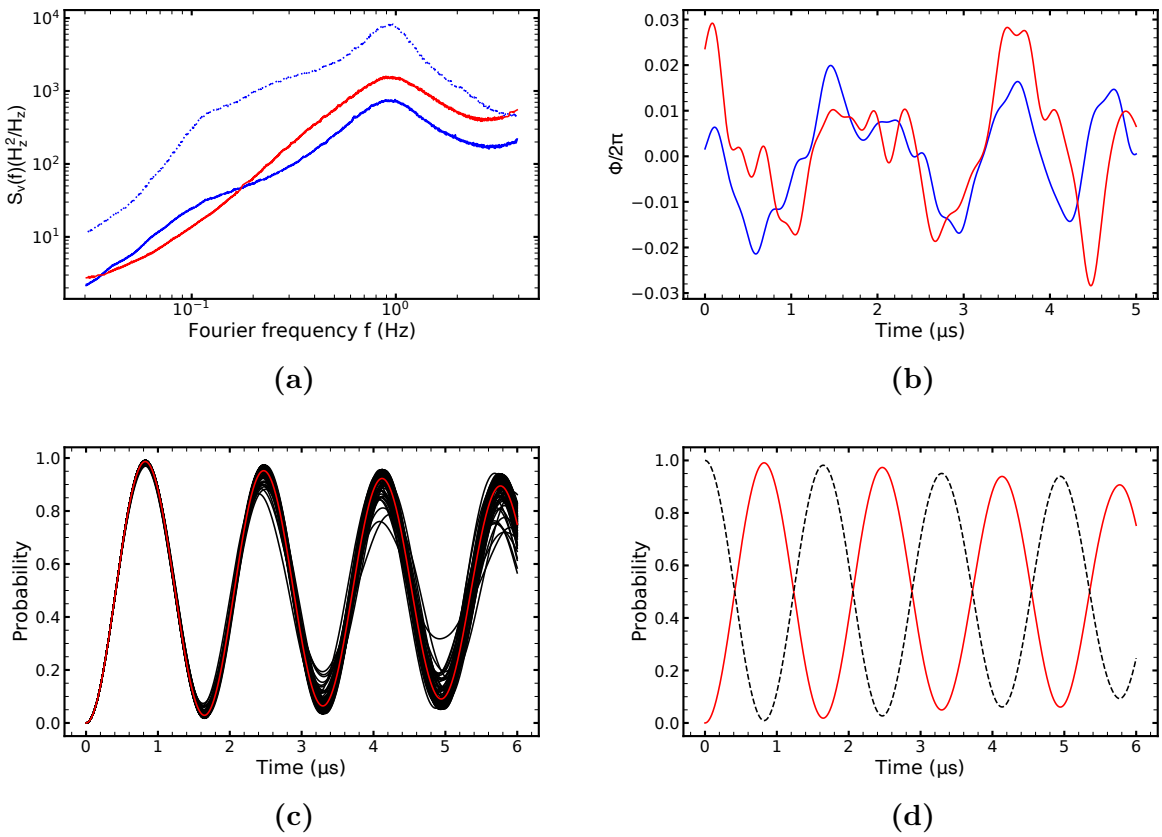

Figure 1.6: Effect of the phase noise on a three–level system. (a) Spectral density of phase noise at 795 nm laser (red), 950 nm laser (blue), and extra noise added in the 950 nm laser (data from Ref. [13]). (b) Example of temporal realizations of phase noise for the two lasers at 950 nm (blue) and 795 nm (red). (c) Average probability of the Rydberg state using Monte Carlo simulation over 100 realizations of the noise (red). The black line represents each realization of the Monte Carlo simulation. (d) Rabi oscillations for the ground state (black dotted) and the Rydberg state (red) of the effective two–level system in the presence of the phase noise. The presence of the phase noise decreases the probability of excitation to the Rydberg state.

For the amplitude noise, the spectral density is obtained from a measurement of the relative intensity noise of the laser. The measured noise spectral density is converted to fluctuations in the driven amplitude field. Figure 1.7 shows the effect of the amplitude noise of the 420 nm laser in our system.

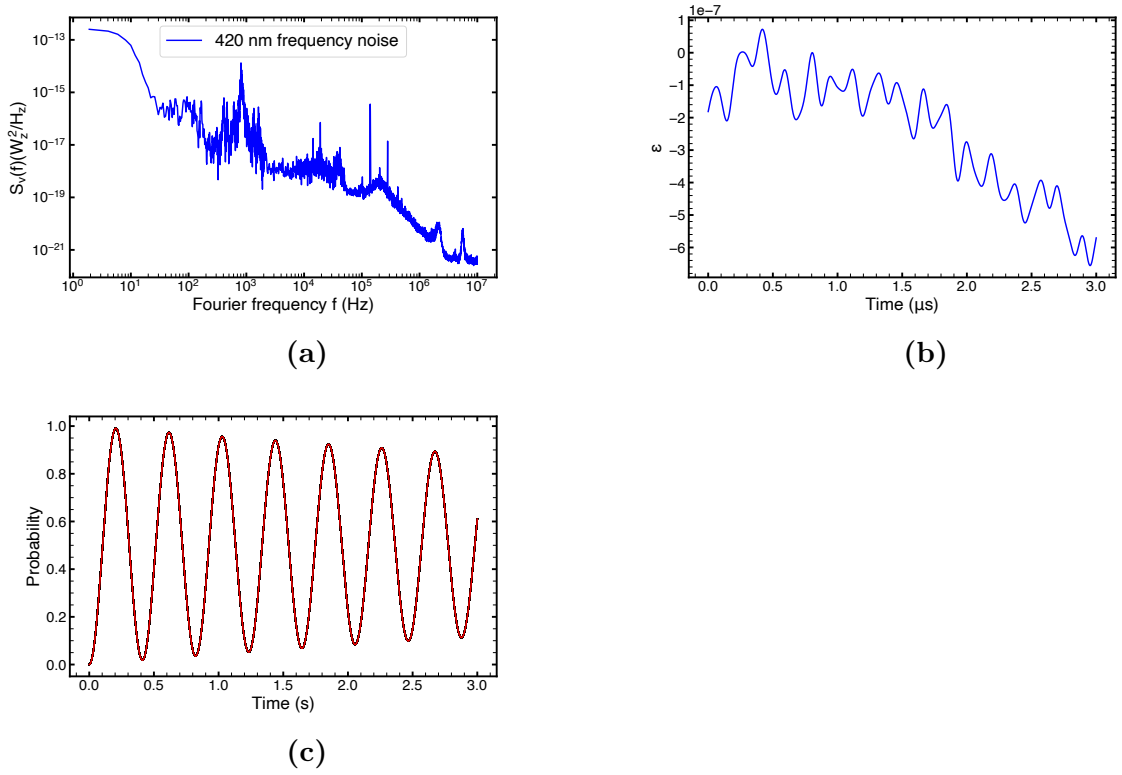

Figure 1.7: Effect of the amplitude noise on a three–level system dynamics. (a) Power spectral density of the amplitude noise at 420 nm. (b) Example of a temporal realization of amplitude noise for the laser at 420 nm (blue). (c) Average probability of the Rydberg state using Monte Carlo simulation over 100 realizations of the noise (red). The presence of the intensity noise in the laser decreases the probability of excitation to the Rydberg state.

These imperfections can be reduced by properly designing the experimental system. For example, the radiative decay from the intermediate state can be reduced by operating at large detunings from the intermediate state or using a direct single–photon transition. The black–body radiation can be suppressed by working in a cryogenic environment. For the Doppler effect, using counter–propagating beams can decrease k_{eff} [14]. Raman sideband cooling of atoms in tweezers can also decrease the magnitude of Doppler shifts [18, 19]. To reduce the decrease in excitation probability caused by the phase and amplitude noise, we can use low–noise laser sources (Titanium–Sapphire) or stabilize the lasers to a high-finesse reference cavity.

In this chapter, we simulated the dynamics of a single rubidium–87 atom excited to a Rydberg state using the Monte Carlo sampling method and the power spectral density of amplitude noise measured on our laser system. After describing our experimental imperfections, we showed that the dynamics of a three–level system can be approximated by the dynamics of an effective two–level system. We simulated the dynamics of the effective two–level system in the presence of amplitude and phase noise on the control lasers. In the next chapter, we will build optimal control pulses to mitigate those imperfections and thus, increase the excitation probability to the Rydberg state.

Chapter 2

Designing an optimal control pulse

The problem is to find a control protocol that maximizes the population $P_r(t)$ of the Rydberg state at some time t given a specific initial state $\rho(0) = |g\rangle\langle g|$. The simplest approach is to drive Rabi oscillations between the ground and Rydberg state using square optical pulses. Because of the large decay rate of the intermediate state, the challenge is to excite an atom from the ground state to the Rydberg state while minimizing the population in the intermediate state.

In this chapter, we use optimal control pulses to counteract dissipation and fluctuations in control parameters. First, we introduce two control protocols to increase the fidelity of excitation of a single Rb–87 atom to a Rydberg state: stimulated Raman adiabatic passage (STIRAP) and superadibatic transitionless driving (SATD). Then, using these protocols, we show that the population of the Rydberg state is maximized. Finally, we design an optimal control pulse to counteract dissipation and fluctuations in control parameters and compare its result to the STIRAP and the SATD protocols.

2.1 Stimulated Raman adiabatic passage (STIRAP)

As mentioned in Chapter 1, transferring the population from the ground state $|g\rangle$ to the Rydberg state $|r\rangle$ is not ideal because of the radiative decay in the intermediate state $|i\rangle$. The goal is to establish a procedure that will allow us to move from the ground state to the Rydberg state without populating the intermediate state such as stimulated Raman adiabatic passage (STIRAP).

Using the STIRAP technique, we first couple the unpopulated states $|i\rangle$ and $|r\rangle$ using the drive field $\Omega_2(t)$. We then couple the intermediate state to the state $|g\rangle$ using the drive field $\Omega_1(t)$. This protocol transfers population of the state $|g\rangle$ into the state $|r\rangle$ without populating the state $|i\rangle$, which is called a dark state [20].

To better understand this protocol, let's consider the time-dependent drive field $\Omega_1(t)$ and $\Omega_2(t)$ acting on the three-level system (Fig. 1.1).

During the STIRAP process, the states $|i\rangle$, $|r\rangle$, $|g\rangle$ are mixed by the two laser fields to form the eigenstates $|b^+\rangle$, $|b^-\rangle$, and $|d\rangle$.

$$
\begin{aligned}
|b^-\rangle &= \sin\theta\cos\phi|g\rangle - \sin\phi|i\rangle + \cos\theta\sin\phi|r\rangle \\
|d\rangle &= \cos\theta|g\rangle - \sin\theta|r\rangle \\
|b^+\rangle &= \sin\theta\sin\phi|g\rangle - \cos\phi|i\rangle + \cos\theta\cos\phi|r\rangle,
\end{aligned}
\tag{2.1}
$$

with respective eigenenergies (Fig. 2.1b)

$$
\begin{aligned}
\lambda_- &= \frac{1}{2}(-\delta_1 - \sqrt{\Delta_1^2 + \Omega_1^2 + \Omega_2^2}\ ) \\
\lambda_0 &= 0 \\
\lambda_+ &= \frac{1}{2}(-\delta_1 + \sqrt{\Delta_1^2 + \Omega_1^2 + \Omega_2^2}\ ),
\end{aligned}
\tag{2.2}
$$

where the mixing angles θ and ϕ are

$$
\begin{aligned}
\tan\theta &= \frac{\Omega_2(t)}{\Omega_1(t)} \\
\tan 2\phi &= -\frac{\sqrt{\Omega_1^2(t) + \Omega_2^2(t)}}{\Delta_1}.
\end{aligned}
\tag{2.3}
$$

In the absence of dissipation, we can then perfectly transfer the population from the ground state to the Rydberg state by respecting the adiabaticity condition

$$
\dot{\theta} \ll \sqrt{\Omega_1^2(t) + \Omega_2^2(t)}. \tag{2.4}
$$

This condition is verified for Gaussian pulses, e.g., by choosing

$$
\begin{aligned}
\Omega_1(t) &= \Omega_0 \exp(-\frac{(t - \Delta t/2)^2}{2\sigma^2}) \\
\Omega_2(t) &= \Omega_0 \exp(-\frac{(t + \Delta t/2)^2}{2\sigma^2}),
\end{aligned}
\tag{2.5}
$$

where σ is the Gaussian pulse width, Ω_0 the maximum Rabi coupling, and Δt the delay between the two lasers (Fig. 2.1a). Figure 2.1c shows the population of the Rydberg state using the STIRAP protocol.

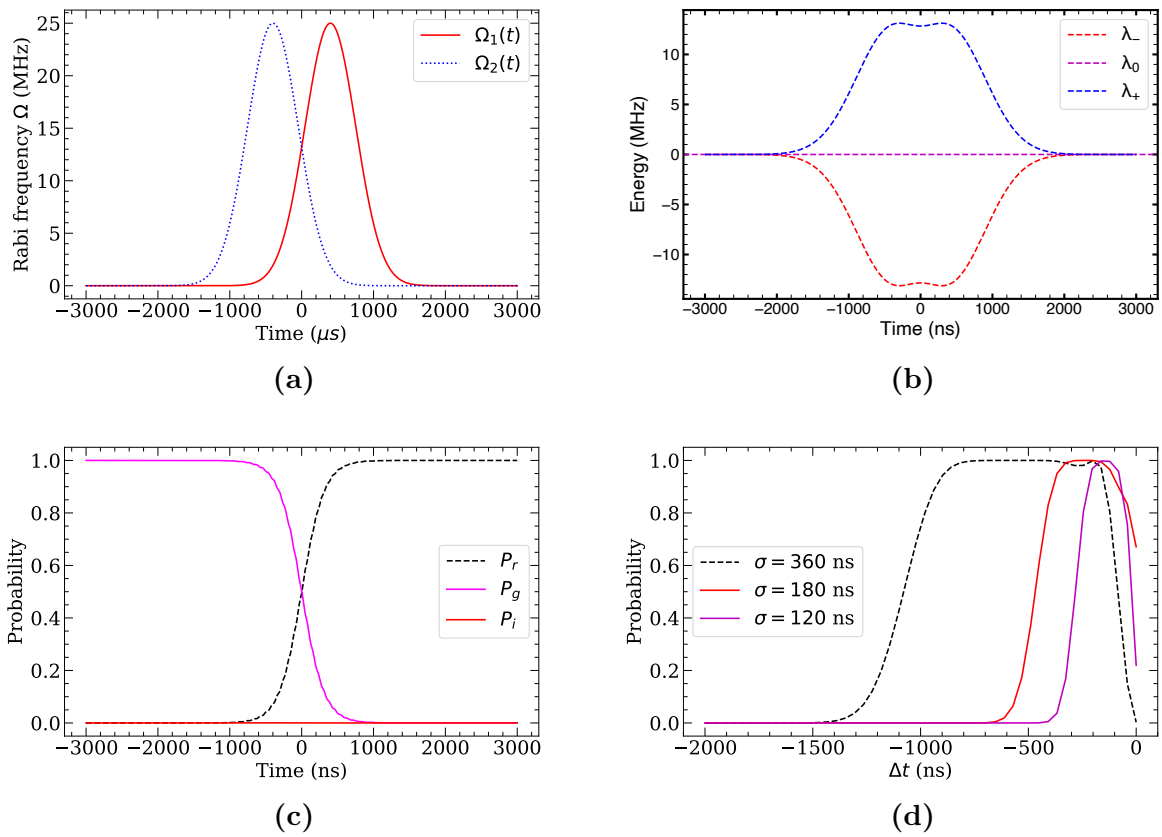

Figure 2.1: Simulation of the three–level system dynamics using STIRAP. (a) Rabi coupling pulse shapes. (b) Energies corresponding to the the STIRAP process. (c) Probability of the Rydberg state (P_r), the intermediate state (P_i), and the ground state (P_g) using STIRAP protocol. Using the STIRAP protocol, there is a small probability to populate the intermediate state. (d) Effect of the pulse widths on the population of the Rydberg state where Δt is the time delay between the two pulses. For $\Delta t < 0$, the pulse acting on the $|i\rangle \leftrightarrow |r\rangle$ transition comes before the pulse acting on the $|g\rangle \leftrightarrow |i\rangle$ transition. The parameters for these plots are $\Delta_1 = 2\pi \times 740$ MHz, $\delta = 0$ kHz, $\Omega_0 = 2\pi \times 25$ MHz, $\sigma = 500$ ns, and $\Delta t = -800$ ns.

Taking into account that there is a small probability to populate the intermediate state due to its decay, the STIRAP protocol could lead to nonadiabatic transitions. Better performance to increase the population of the Rydberg state can be achieved by minimizing nonadiabatic transitions.

2.2 Superadiabatic transitionless driving (SATD)

Dykhne–Davis–Pechukas have shown a technique for deriving the transition probability in the near adiabatic regime [21]. The probability for nonadiabatic transition is

$$P \approx e^{-2ImD(t_0)}, \tag{2.6}$$

where

$$D(t_0) = \int_0^{t_0} \epsilon(t) dt \tag{2.7}$$

is an integral over the splitting $\epsilon(t) = \sqrt{\Omega_{eff}(t)^2 + \Delta_{AC}(t)^2}$ between eigenenergies of Eq. (2.2) and t_0 is the transition point. To optimize the adiabatic passage between two states, we choose $\Omega_{eff}(t)$ and Δ_{AC} [22] such that

$$\epsilon(t) = \sqrt{\Omega_{eff}(t)^2 + \Delta_{AC}(t)^2} = \text{constant}. \tag{2.8}$$

The condition for our effective two-level system is

$$\Omega_{eff}(t)^2 + \Delta_{AC}(t)^2 = [\frac{\Omega_1(t)^2 + \Omega_2(t)^2}{4\Delta_1}]^2 = \text{constant}. \tag{2.9}$$

We choose the following parameterization

$$\begin{aligned} \Omega_1(t) &= \Omega \sin[\frac{\pi}{2} f(t)] \\ \Omega_2(t) &= \Omega \cos[\frac{\pi}{2} f(t)], \end{aligned} \tag{2.10}$$

where $f(t)$ is an arbitrary increasing function $0 = f(-\infty) \leq f(t) \leq f(\infty) = 1$. Eq. (2.8) requires that Ω must be constant, which is not physically feasible. To overcome this unphysical condition, Vasilev introduced a mask function $F(t)$ [23] in Eq. (2.10) and obtained

$$\begin{aligned} \Omega_1(t) &= \Omega_0 F(t) \sin[\frac{\pi}{2} f(t)] \\ \Omega_2(t) &= \Omega_0 F(t) \cos[\frac{\pi}{2} f(t)], \end{aligned} \tag{2.11}$$

where $F(t)$ is chosen as the hypergaussian function defined as

$$F(t) = e^{(t/T_0)^{2n}}. \tag{2.12}$$

Taking into account the adiabaticity condition

$$|\dot{\theta}(t)| \ll |\epsilon(t)|, \tag{2.13}$$

we can choose $f(t)$ as

$$f(t) = \frac{1}{1 + e^{-(\lambda t/T)}}. \tag{2.14}$$

For $n = 1$, we have a Gaussian pulse with the following pulse shapes

$$\begin{aligned} \Omega_1(t) &= \Omega_0 e^{-(t-\tau/2)/T^2} \\ \Omega_2(t) &= \Omega_0 e^{-(t+\tau/2)/T^2}, \end{aligned} \tag{2.15}$$

where τ is the pulse delay. Figure 2.2 shows the dynamics of the effective two–level system using the SATD protocol.

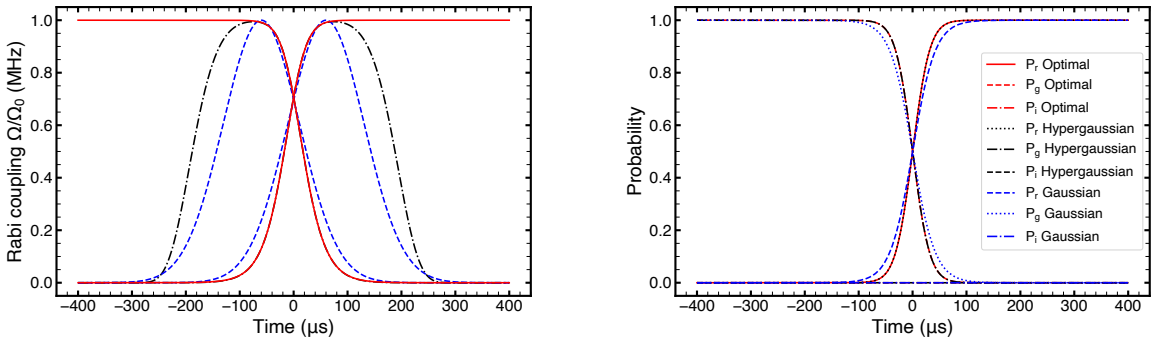

(a) **(b)**

Figure 2.2: Simulation of the three–level system dynamics using SATD. (a) Pulse shapes for different time–dependent Rabi coupling. Ideally optimized pulse shapes (red solid line), which obey the optimization condition given by the Eq. 2.13 for all times t. Pulse shapes with hypergaussian mask (black dashdot line) (Eq. 2.12), with $n = 3$, $\lambda = 4$, $T = 100$ ns and $T_0 = 2T$. Gaussian pulses (blue dash line) with pulse delay $\tau = 1.2T$. (b) Comparison of the population of the Rydberg state using different pulse shapes described in SATD protocol. Although the Gaussian pulses are faster, the optimal and the hypergaussian pulses show high probability of reaching the Rydberg state. The parameters for these plots are, $\Delta_1 = 2\pi \times 740$ MHz, $\delta = 0$ kHz, $\Omega_0 = 2\pi \times 25$ MHz, $\sigma = 500$ ns, $\Delta_t = 800$ ns.

We showed how certain control protocols with shaped pulses could increase the probability to reach the Rydberg state. In the next part, we will build an optimal control using TensorFlow to minimize the infidelity of the Rydberg excitation process.

2.3 Quantum Optimal Control (QOC)

Optimizing the fidelity of the Rydberg state requires finding the control parameters that will maximize the population of the Rydberg state. We use Δ_1, Ω_1, and the pulse duration as our control parameters. Our optimization is done at time $T = 2\pi/\Omega_{eff}$. The number of Rabi flops Q driven at rate Ω_{eff} during the effective Rydberg lifetime $\tau = 1/\Gamma_{eff}$ is

$$\begin{aligned} Q &= \tau/T \\ &\approx \frac{1}{\Gamma_{eff}} \frac{\Omega_{eff}}{2\pi} \\ &\approx \frac{\frac{1}{2\pi}\frac{\Omega_1\Omega_2}{2\Delta_1}}{\Gamma_r + \Gamma_i \frac{\Omega_1^2}{4\Delta_1^2}}. \end{aligned} \tag{2.16}$$

We numerically maximize Q (Eq. 2.16) over Δ_1 (Figure 2.3a) to obtain

$$Q_{max} = \frac{1}{4\pi} \frac{\Omega_2}{\sqrt{\Gamma_r \Gamma_i}}, \tag{2.17}$$

at

$$\Delta_1^* = \sqrt{\frac{\Gamma_i}{\Gamma_r}\frac{\Omega_1^2}{4}}. \tag{2.18}$$

We find the detuning Δ_1 at which the excitation probability to the Rydberg state is maximum by maximizing numerically the number of Rabi flops (Figure 2.3).

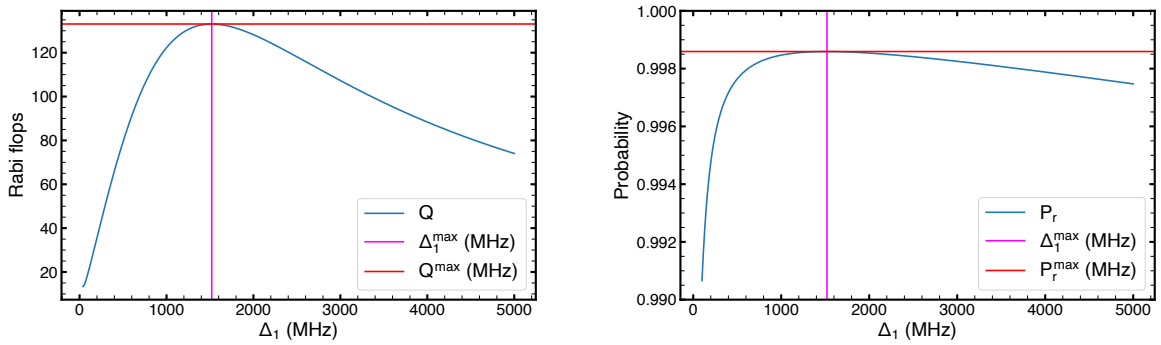

(a) **(b)**

Figure 2.3: Optimized π pulses parameters. (a) Rabi flops as a function of Δ_1. (b) Probability of the Rydberg state as a function of Δ_1. The highest probability of the Rydberg state is obtained for $\Delta_1 = \Delta_1^* = 1520.3$ MHz.

Given the initial state (ground state) and the target state (Rydberg state) of our system, we use TensorFlow to build an optimal pulse that will maximize the fidelity of the Rydberg state and be robust against fluctuating control parameters. The algorithm consists of first, defining a set of control parameters (pulse duration, the drive–field Ω_1, the detuning Δ_1), the sources of noise (amplitude noise on the drive–field), a target state (Rydberg state), and the pulse segments that define the number of steps of the optimizer. Then, we create a pulse (Fig. 2.4a) that maximizes the fidelity of the Rydberg state using the Adams optimizer. This optimizer allows us to create a pulse that is robust against fluctuations in control parameters (Fig. 2.4b, Fig. 2.4c). Figure 2.4 shows the comparision of the excitation probability to the Rydberg state using the STIRAP, SATD, and QOC protocols.

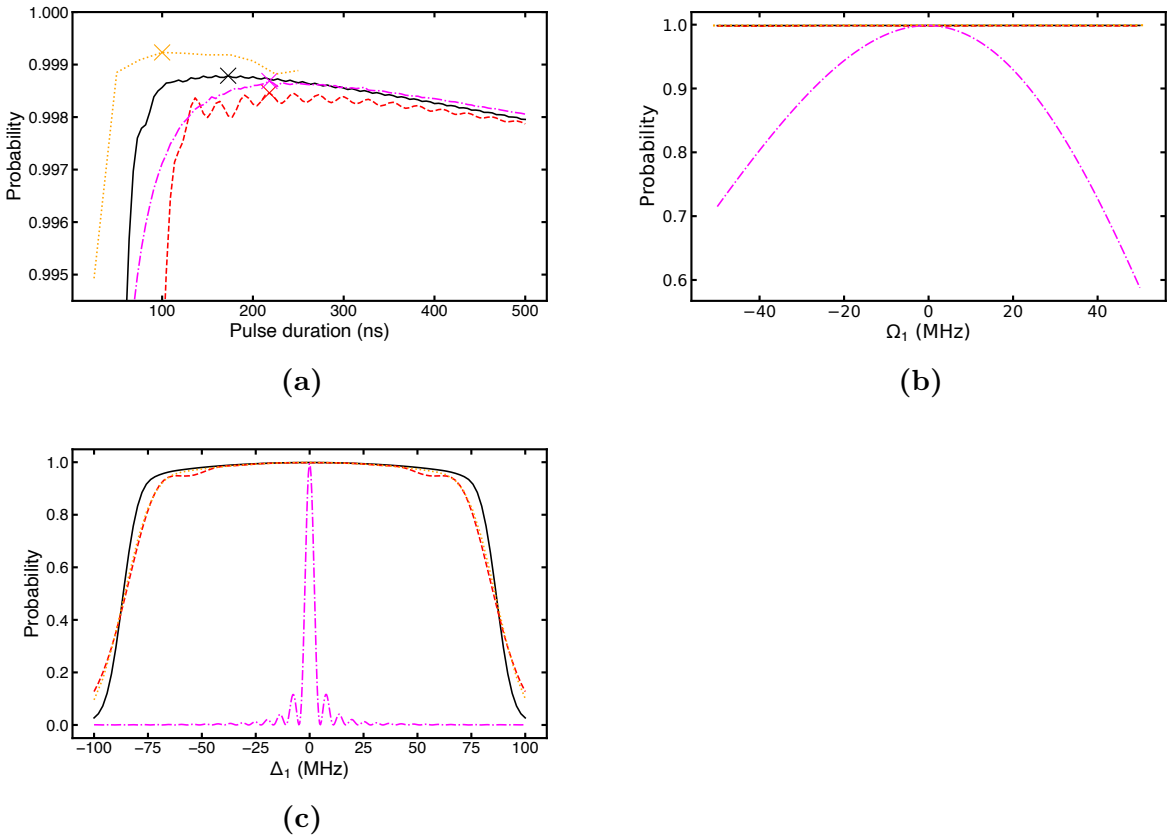

Figure 2.4: Excitation probability for different control protocols: π pulses (pink dashdot line), STIRAP (red dash line), SATD (black solid line), and QOC (yellow dotted line). (a) The maximum population of the Rydberg state is obtained using quantum optimal control (QOC) (yellow cross). (b-c) The control pulses for STIRAP (red dash line), SATD (black solid line), and QOC (yellow dotted line) are robust against amplitude and frequency fluctuations. At $t = 175\ ns$, the second derivative of the infidelity using STIRAP, SATD and QOC protocols with respect to the amplitude's fluctuations tends to zero. The simulation parameters are $\delta = 0$, $\Omega_1 = 2\pi \times 174$ MHz, $\Omega_2 = 2\pi \times 115$ MHz, $t_f = 0.175\ \mu$s, $\sigma = t_f/6$, $\tau = \sigma \times 1.2$, $\lambda = 2$.

In this chapter, we built upon the Gaussian-like pulses of the STIRAP and SATD protocols to synthesize novel quantum optimal control pulses that achieve a greater excitation probability to the Rydberg state in less time, while being robust against fluctuations in control parameters. First, we used the STIRAP and SATD protocols to increase the fidelity of excitation of a single Rb–87 atom to a Rydberg state. Then, we extended those protocols using quantum optimal control. Finally, we compared their robustness against the detuning Δ_1 from the intermediate state. We concluded that quantum optimal control provides control protocols with superior performance that are fast and robust against fluctuations in control parameters.

Chapter 3

Conclusion

In this thesis, we designed an optimal control pulse to excite a rubidium–87 atom to the Rydberg state in the presence of dissipative physical processes and fluctuating control parameters.

First, we simulated the dynamics of a single Rb–87 atom excited to the Rydberg state in the presence of imperfections and showed that a three–level system could be approximated by an effective two–level system in the case of a large detuning from the intermediate state. Then, we used the STIRAP and SATD protocols to minimize the population of the intermediate state and the nonadiabatic transitions respectively. Finally, we built a quantum optimal control protocol to mitigate the effect of physical imperfections and fluctuations in control parameters. We found the parameters that maximize the Rabi flops and the population of the Rydberg state using π pulses. Then, we designed an optimal control pulse that minimized the infidelity of the Rydberg state and compared its performance against the STIRAP and SATD protocols. We saw that QOC gives the highest excitation probability to the Rydberg state, while being faster ($t \ll 400$ ns) and robust against fluctuations in control parameters.

These results will be useful to experimentally model a three-level system and measure the population of the Rydberg state in the presence of dissipative physical parameters and fluctuating control parameters. Increasing the population of the Rydberg state will help improving the performance of quantum simulators based on arrays of Rydberg atoms for applications in quantum information processing.

For the Future work, we plan to demonstrate these results experimentally, exploit quantum optimal control to design efficient spectroscopy techniques to sample and reconstruct non–markovian noise acting on two–photon transitions, and extend these results from a state–to–state transfer problem defined for a single quantum system to a quantum gate synthesis problem defined for a many–body quantum system.

References

[1] A. Browaeys and T. Lahaye, "Many-body physics with individually controlled rydberg atoms," *Nature Physics*, pp. 1–11, 2020.

[2] D. Barredo, V. Lienhard, S. De Leseleuc, T. Lahaye, and A. Browaeys, "Synthetic three-dimensional atomic structures assembled atom by atom," *Nature*, vol. 561, no. 7721, pp. 79–82, 2018.

[3] H. Bernien, S. Schwartz, A. Keesling, H. Levine, A. Omran, H. Pichler, S. Choi, A. S. Zibrov, M. Endres, M. Greiner, *et al.*, "Probing many-body dynamics on a 51-atom quantum simulator," *Nature*, vol. 551, no. 7682, p. 579, 2017.

[4] R. Blatt and C. F. Roos, "Quantum simulations with trapped ions," *Nature Physics*, vol. 8, no. 4, pp. 277–284, 2012.

[5] M. Endres, H. Bernien, A. Keesling, H. Levine, E. R. Anschuetz, A. Krajenbrink, C. Senko, V. Vuletic, M. Greiner, and M. D. Lukin, "Atom-by-atom assembly of defect-free one-dimensional cold atom arrays," *Science*, vol. 354, no. 6315, pp. 1024–1027, 2016.

[6] H. Levine, A. Keesling, G. Semeghini, A. Omran, T. T. Wang, S. Ebadi, H. Bernien, M. Greiner, V. Vuletić, H. Pichler, and et al., "Parallel implementation of high-fidelity multiqubit gates with neutral atoms," *Physical Review Letters*, vol. 123, Oct 2019.

[7] T. L. Nguyen, J.-M. Raimond, C. Sayrin, R. Cortinas, T. Cantat-Moltrecht, F. Assemat, I. Dotsenko, S. Gleyzes, S. Haroche, G. Roux, *et al.*, "Towards quantum simulation with circular rydberg atoms," *Physical Review X*, vol. 8, no. 1, p. 011032, 2018.

[8] P. Schauss, "Quantum simulation of transverse ising models with rydberg atoms," *Quantum Science and Technology*, vol. 3, no. 2, p. 023001, 2018.

[9] D. Schönleber, A. Eisfeld, M. Genkin, S. Whitlock, and S. Wüster, "Quantum simulation of energy transport with embedded rydberg aggregates," *Physical review letters*, vol. 114, no. 12, p. 123005, 2015.

[10] F. M. Surace, P. P. Mazza, G. Giudici, A. Lerose, A. Gambassi, and M. Dalmonte, "Lattice gauge theories and string dynamics in rydberg atom quantum simulators," *Physical Review X*, vol. 10, no. 2, p. 021041, 2020.

[11] L. Theis, F. Motzoi, F. Wilhelm, and M. Saffman, "High-fidelity rydberg-blockade entangling gate using shaped, analytic pulses," *Physical Review A*, vol. 94, no. 3, p. 032306, 2016.

[12] S. D. L. de Kerouara, *Quantum simulation of spin models with assembled arrays of Rydberg atoms*. PhD thesis, Université Paris-Saclay, 2018.

[13] S. De Léséleuc, D. Barredo, V. Lienhard, A. Browaeys, and T. Lahaye, "Analysis of imperfections in the coherent optical excitation of single atoms to rydberg states," *Physical Review A*, vol. 97, no. 5, p. 053803, 2018.

[14] H. Levine, A. Keesling, A. Omran, H. Bernien, S. Schwartz, A. S. Zibrov, M. Endres, M. Greiner, V. Vuletić, and M. D. Lukin, "High-fidelity control and entanglement of rydberg-atom qubits," *Physical review letters*, vol. 121, no. 12, p. 123603, 2018.

[15] A. Omran, H. Levine, A. Keesling, G. Semeghini, T. T. Wang, S. Ebadi, H. Bernien, A. S. Zibrov, H. Pichler, S. Choi, *et al.*, "Generation and manipulation of schrodinger cat states in rydberg atom arrays," *arXiv preprint arXiv:1905.05721*, 2019.

[16] A. Browaeys, D. Barredo, and T. Lahaye, "Experimental investigations of dipole–dipole interactions between a few rydberg atoms," *Journal of Physics B: Atomic, Molecular and Optical Physics*, vol. 49, no. 15, p. 152001, 2016.

[17] A. Kramida, Yu. Ralchenko, J. Reader, and and NIST ASD Team. NIST Atomic Spectra Database (ver. 5.8), [Online]. Available: `https://physics.nist.gov/asd` [2020, December 7]. National Institute of Standards and Technology, Gaithersburg, MD., 2020.

[18] J. D. Thompson, T. Tiecke, A. S. Zibrov, V. Vuletić, and M. D. Lukin, "Coherence and raman sideband cooling of a single atom in an optical tweezer," *Physical Review Letters*, vol. 110, no. 13, p. 133001, 2013.

[19] A. M. Kaufman, B. J. Lester, and C. A. Regal, "Cooling a single atom in an optical tweezer to its quantum ground state," *Physical Review X*, vol. 2, no. 4, p. 041014, 2012.

[20] P. Marte, P. Zoller, and J. L. Hall, "Coherent atomic mirrors and beam splitters by adiabatic passage in multilevel systems," *Physical Review A*, vol. 44, no. 7, p. R4118, 1991.

[21] V. Benderskii, E. Vetoshkin, and E. Kats, "Instanton versus traditional wkb approach to the landau-zener problem," *Journal of Experimental and Theoretical Physics*, vol. 97, no. 2, pp. 232–258, 2003.

[22] S. Guérin, S. Thomas, and H. Jauslin, "Optimization of population transfer by adiabatic passage," *Physical Review A*, vol. 65, no. 2, p. 023409, 2002.

[23] G. Vasilev, A. Kuhn, and N. Vitanov, "Optimum pulse shapes for stimulated raman adiabatic passage," *Physical Review A*, vol. 80, no. 1, p. 013417, 2009.

[24] N. Robinson, "Cold atoms bear a quantum scar," *Physics*, vol. 11, p. 105, 2018.

[25] S. de Léséleuc, V. Lienhard, P. Scholl, D. Barredo, S. Weber, N. Lang, H. P. Büchler, T. Lahaye, and A. Browaeys, "Experimental realization of a symmetry protected topological phase of interacting bosons with rydberg atoms," *arXiv preprint arXiv:1810.13286*, 2018.

[26] H. Labuhn, D. Barredo, S. Ravets, S. De Léséleuc, T. Macrì, T. Lahaye, and A. Browaeys, "Tunable two-dimensional arrays of single rydberg atoms for realizing quantum ising models," *Nature*, vol. 534, no. 7609, p. 667, 2016.

[27] V. Lienhard, S. De Léséleuc, D. Barredo, T. Lahaye, A. Browaeys, M. Schuler, L.-P. Henry, and A. M. Läuchli, "Observing the space-and time-dependent growth of correlations in dynamically tuned synthetic ising models with antiferromagnetic interactions," *Physical Review X*, vol. 8, no. 2, p. 021070, 2018.

[28] H. Kim, Y. Park, K. Kim, H.-S. Sim, and J. Ahn, "Detailed balance of thermalization dynamics in rydberg-atom quantum simulators," *Physical review letters*, vol. 120, no. 18, p. 180502, 2018.

[29] F. Nogrette, H. Labuhn, S. Ravets, D. Barredo, L. Béguin, A. Vernier, T. Lahaye, and A. Browaeys, "Single-atom trapping in holographic 2d arrays of microtraps with arbitrary geometries," *Physical Review X*, vol. 4, no. 2, p. 021034, 2014.

[30] N. Wiebe, C. Granade, C. Ferrie, and D. G. Cory, "Hamiltonian learning and certification using quantum resources," *Physical review letters*, vol. 112, no. 19, p. 190501, 2014.

[31] H. J. Metcalf and P. Van der Straten, "Laser cooling and trapping of neutral atoms," *The Optics Encyclopedia: Basic Foundations and Practical Applications*, 2007.

[32] A. Mitra, M. J. Martin, G. W. Biedermann, A. M. Marino, P. M. Poggi, and I. H. Deutsch, "Robust molmer-sorenson gate for neutral atoms using rapid adiabatic rydberg dressing," *arXiv preprint arXiv:1911.04045*, 2019.

[33] V. M. Frey, S. Mavadia, L. M. Norris, W. de Ferranti, D. Lucarelli, L. Viola, and M. J. Biercuk, "Application of optimal band-limited control protocols to quantum noise sensing," *Nature Communications*, vol. 8, Dec 2017.

[34] T. J. Green, J. Sastrawan, H. Uys, and M. J. Biercuk, "Arbitrary quantum control of qubits in the presence of universal noise," *New Journal of Physics*, vol. 15, p. 095004, Sep 2013.

[35] L. M. Norris, D. Lucarelli, V. M. Frey, S. Mavadia, M. J. Biercuk, and L. Viola, "Optimally band-limited spectroscopy of control noise using a qubit sensor," *Physical Review A*, vol. 98, Sep 2018.

[36] D. S. Weiss and M. Saffman, "Quantum computing with neutral atoms," *Physics Today*, vol. 70, no. 7, 2017.

[37] J. I. Cirac and P. Zoller, "A scalable quantum computer with ions in an array of microtraps," *Nature*, vol. 404, no. 6778, pp. 579–581, 2000.

[38] S. Yelin, R. Cote, and T. Calarco, "Quantum computing with polar molecules," *APS*, vol. 37, pp. G1–143, 2006.

[39] V. Privman, D. Mozyrsky, and I. D. Vagner, "Quantum computing with spin qubits in semiconductor structures," *Computer physics communications*, vol. 146, no. 3, pp. 331–338, 2002.

[40] J. Preskill, "Quantum computing in the nisq era and beyond," *Quantum*, vol. 2, p. 79, 2018.

[41] D. G. Cory, M. D. Price, and T. F. Havel, "Nuclear magnetic resonance spectroscopy: An experimentally accessible paradigm for quantum computing," *Physica D: Nonlinear Phenomena*, vol. 120, no. 1-2, pp. 82–101, 1998.

[42] J. Franson, B. Jacobs, and T. Pittman, "Quantum computing using single photons and the zeno effect," *Physical Review A*, vol. 70, no. 6, p. 062302, 2004.

[43] S. De Léséleuc, S. Weber, V. Lienhard, D. Barredo, H. P. Büchler, T. Lahaye, and A. Browaeys, "Accurate mapping of multilevel rydberg atoms on interacting spin-1/2 particles for the quantum simulation of ising models," *Physical review letters*, vol. 120, no. 11, p. 113602, 2018.

[44] A. Baksic, H. Ribeiro, and A. A. Clerk, "Speeding up adiabatic quantum state transfer by using dressed states," *Physical review letters*, vol. 116, no. 23, p. 230503, 2016.

[45] J. Bylander, S. Gustavsson, F. Yan, F. Yoshihara, K. Harrabi, G. Fitch, D. G. Cory, Y. Nakamura, J.-S. Tsai, and W. D. Oliver, "Dynamical decoupling and noise spectroscopy with a superconducting flux qubit," *arXiv preprint arXiv:1101.4707*, 2011.

[46] G. A. Álvarez and D. Suter, "Measuring the spectrum of colored noise by dynamical decoupling," *Physical review letters*, vol. 107, no. 23, p. 230501, 2011.

[47] C. Ferrie, C. Granade, G. Paz-Silva, and H. M. Wiseman, "Bayesian quantum noise spectroscopy," *New Journal of Physics*, vol. 20, no. 12, p. 123005, 2018.

[48] A. A. Clerk, M. H. Devoret, S. M. Girvin, F. Marquardt, and R. J. Schoelkopf, "Introduction to quantum noise, measurement, and amplification," *Reviews of Modern Physics*, vol. 82, no. 2, p. 1155, 2010.

[49] O. Astafiev, Y. A. Pashkin, Y. Nakamura, T. Yamamoto, and J.-S. Tsai, "Quantum noise in the josephson charge qubit," *Physical review letters*, vol. 93, no. 26, p. 267007, 2004.

[50] D. Slepian and H. O. Pollak, "Prolate spheroidal wave functions, fourier analysis and uncertainty—i," *Bell System Technical Journal*, vol. 40, no. 1, pp. 43–63, 1961.

[51] D. J. Thomson, "Spectrum estimation and harmonic analysis," *Proceedings of the IEEE*, vol. 70, no. 9, pp. 1055–1096, 1982.